Tuning transport coefficients of monolayer $MoSi_2N_4$ with biaxial strain

Xiao-Shu Guo[1] and San-Dong Guo[2,3]

[1]*Xi'an University of Posts and Telecommunications, Xi'an 710121, China*
[2]*School of Electronic Engineering, Xi'an University of Posts and Telecommunications, Xi'an 710121, China and*
[3]*Key Laboratory of Advanced Semiconductor Devices and Materials,*
Xi'an University of Posts and Telecommunications, Xi'an 710121, China

Experimentally synthesized $MoSi_2N_4$ (Science 369, 670-674 (2020)) is a piezoelectric semiconductor. Here, we systematically study the large biaxial (isotropic) strain effects (0.90 to 1.10) on electronic structures and transport coefficients of monolayer $MoSi_2N_4$ by density functional theory (DFT). With a/a_0 from 0.90 to 1.10, the energy band gap firstly increases, and then decreases, which is due to transformation of conduction band minimum (CBM). Calculated results show that the $MoSi_2N_4$ monolayer is mechanically stable in considered strain range. It is found that the spin-orbital coupling (SOC) effects on Seebeck coefficient depend on the strain. In unstrained $MoSi_2N_4$, the SOC has neglected influence on Seebeck coefficient. However, the SOC can produce important influence on Seebeck coefficient, when the strain is applied, for example 0.96 strain. The compressive strain can change relative position and numbers of conduction band extrema (CBE), and then the strength of conduction bands convergence can be enhanced, to the benefit of n-type ZT_e. Only about 0.96 strain can effectively improve n-type ZT_e. Our works imply that strain can effectively tune the electronic structures and transport coefficients of monolayer $MoSi_2N_4$, and can motivate farther experimental exploration.

I. INTRODUCTION

The successful exfoliation of graphene[1] induces increasing attention on two-dimensional (2D) materials. Many of them have semiconducting behaviour, which has various potential application in electronics, optoelectronics and piezoelectronics[2–5]. Their electronic structures, heat transport and piezoelectric properties have been widely investigated[6–16]. It has been proved that the strain can effectively tune electronic structures, transport and piezoelectric properties of 2D materials[15–23], which shows great potential for better use in the nanoelectronic, thermoelectric and piezoelectric applications. For example, both compressive and tensile strain can induce the semiconductor to metal transition in monolayer MoS_2[17]. In many transition metal dichalchogenides (TMD) monolayers, the power factor can be enhanced by strain due to bands converge[15,16,18]. With increased tensile strain, the lattice thermal conductivity shows monotonous decrease, up-and-down and jump behavior with similar penta-structures[19]. Strain can also improve the piezoelectric strain coefficient by tuning the elastic and piezoelectric stress coefficients[20–23].

Recently, the layered 2D $MoSi_2N_4$ and WSi_2N_4 have been experimentally achieved by chemical vapor deposition (CVD)[24]. The septuple-atomic-layer MA_2Z_4 monolayers with twelve different structures are constructed by intercalating MoS_2-type MZ_2 monolayer into InSe-type A_2Z_2 monolayer[25]. The 66 thermodynamically and dynamically stable MA_2Z_4 are predicted by the first principle calculations. They can be common semiconductor, half-metal ferromagnetism or spin-gapless semiconductor (SGS), Ising superconductor and topological insulator,
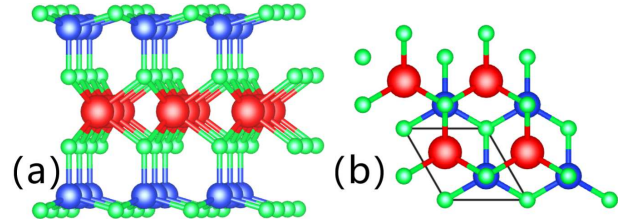

FIG. 1. (Color online) The crystal structure of monolayer $MoSi_2N_4$ ((a) side view and (b) top view). The primitive cell is are marked by black line, and the large red balls represent Mo atoms, and the middle blue balls for Si atoms, and the small green balls for N atoms.

which depends on the number of valence electrons[25]. We predict intrinsic piezoelectricity in monolayer MA_2Z_4[26], which means that MA_2Z_4 family may have potential application in piezoelectric field. Structure effect on intrinsic piezoelectricity in monolayer MSi_2N_4 (M=Mo and W) has also been reported by the first principle calculations[27]. By applied strain, the VSi_2P_4 monolayer undergoes ferromagnetic metal (FMM) to SGS to ferromagnetic semiconductor (FMS) to SGS to ferromagnetic half-metal (FMHM) with increasing strain[28]. Some materials of MA_2Z_4 lack inversion symmetry with a strong SOC effect, which are expected to exhibit rich spin-valley physics[25]. The valley-dependent properties of monolayer $MoSi_2N_4$, WSi_2N_4 and $MoSi_2As_4$ have been predicted by the first-principles calculations[25,29,30]. Recently, Janus 2D monolayer in the new septuple-atomic-layer 2D MA_2Z_4 family has been achieved[31], which shows Rashba spin splitting and out-of-plane piezoelectric polarizations.
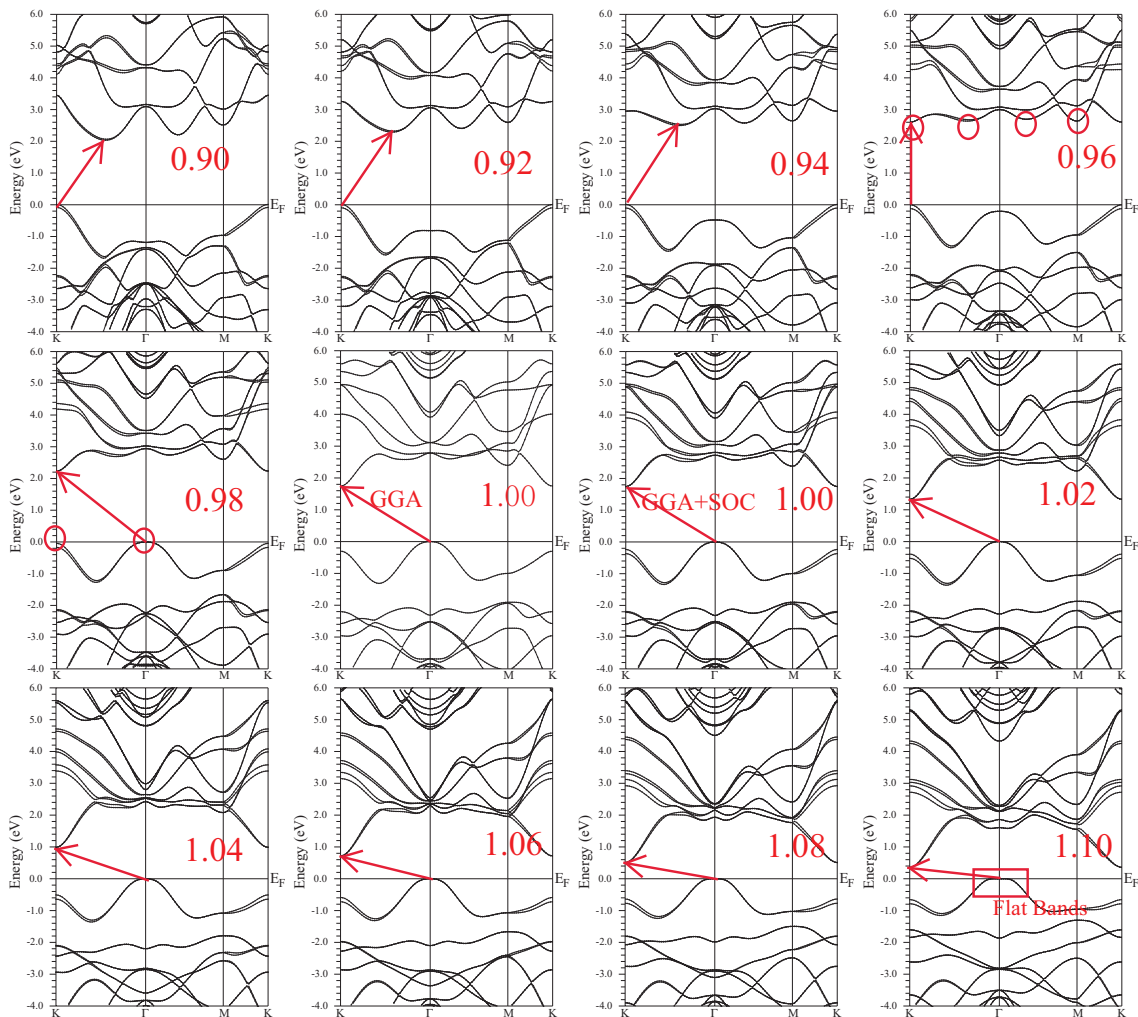
FIG. 2. (Color online) The energy band structures of monolayer $MoSi_2N_4$ using GGA+SOC with the application of biaxial strain (-10% to 10%), and the unstrained energy band using GGA. The VBM and CBM are marked by arrows. At 0.96 (0.98) strain, four CBE (two VBE) are marked by ellipse.

In nanoscale devices, the residual strain usually exists in real applications[32]. In our previous work, the small strain effects (0.96 to 1.04) on piezoelectric coefficients of monolayer $MoSi_2N_4$ have been investigated[26]. In this work, the large (0.90 to 1.10) biaxial strain-tuned electronic structures and transport coefficients of monolayer $MoSi_2N_4$ are studied by the first principle calculations. With a/a_0 from 0.90 to 1.10, the energy band gap of monolayer $MoSi_2N_4$ firstly increases, and then decreases. In n-type doping, the Seebeck coefficient S can be effectively enhanced by applying compressive strain, and then the ZT_e can be improved. The tensile strain can induce flat valence bands around the Γ point near the Fermi level, producing large p-type S. Therefore, our works give an experimental proposal to improve transport coefficients of monolayer $MoSi_2N_4$.

The rest of the paper is organized as follows. In the next section, we shall give our computational details and methods about transport coefficients. In the third and fourth sections, we will present main results of monolayer $MoSi_2N_4$ about strain-tuned electronic structures and transport coefficients. Finally, we shall give our conclusions in the sixth section.

II. COMPUTATIONAL DETAIL

To avoid interactions between two neighboring images, a vacuum spacing of more than 32 Å along the z direction is added to construct monolayer $MoSi_2N_4$. The elastic stiffness tensor C_{ij} are calculated by using strain-stress relationship (SSR), which are performed by using the VASP code[33–35] within the framework of DFT[36]. A kinetic cutoff energy of 500 eV is adopted, and we use the popular generalized gradient approximation of Perdew, Burke and Ernzerh of (GGA-PBE)[37] as the exchange-correlation potential to calculate elastic and electronic properties. The total energy convergence criterion is set
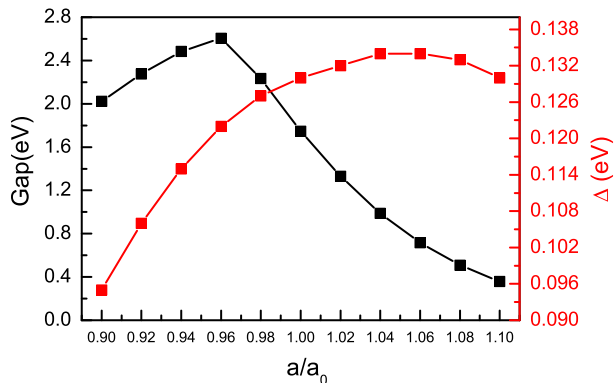
FIG. 3. (Color online) For $MoSi_2N_4$ monolayer, the energy band gap and spin-orbit splitting value Δ at K point using GGA+SOC as a function of strain.

to 10^{-8} eV, and the Hellmann-Feynman forces on each atom are less than 0.0001 eV.Å^{-1}. The Brillouin zone (BZ) sampling is done using a Monkhorst-Pack mesh of $15\times15\times1$ for elastic constants C_{ij}. The 2D elastic coefficients C_{ij}^{2D} have been renormalized by the the length of unit cell along z direction (Lz): $C_{ij}^{2D}=LzC_{ij}^{3D}$.

The electronic transport coefficients of $MoSi_2N_4$ monolayer are calculated through solving Boltzmann transport equations within the constant scattering time approximation (CSTA), which is performed by BoltzTrap[38] code. To include the SOC, a full-potential linearized augmented-plane-waves method is used to calculate the energy bands of $MoSi_2N_4$ monolayer, as implemented in the WIEN2k package[39]. To attain accurate transport coefficients, a $35 \times35\times 1$ k-point meshes is used in the first BZ for the energy band calculation, make harmonic expansion up to $l_{max} = 10$ in each of the atomic spheres, and set $R_{mt} * k_{max} = 8$.

III. ELECTRONIC STRUCTURES

The $MoSi_2N_4$ monolayer can be considered as the insertion of the 2H MoS_2-type MoN_2 monolayer into the α-InSe-type Si_2N_2, and the side and top views of the structure of the $MoSi_2N_4$ monolayer are plotted in Figure 1. The structure breaks the inversion symmetry, but preserves a horizontal mirror corresponding to the plane of the Mo layer. This leads to that $MoSi_2N_4$ monolayer only has in-plane piezoelectric response, and has not out-of-plane piezoelectric polarizations. Using optimized lattice constants[26], the energy bands of $MoSi_2N_4$ monolayer using GGA and GGA+SOC are shown in Figure 2, and exhibit both the indirect band gaps with valence band maximum (VBM) at Γ point and CBM at K point. Due to lacking inversion symmetry and containing the heavy element Mo, there exists a SOC induced spin splitting of about 0.13 eV near the Fermi level in the valence bands at K point. This may provide a platform for spin-valley physics[25,29,30], but the VBM is not at K point, which can
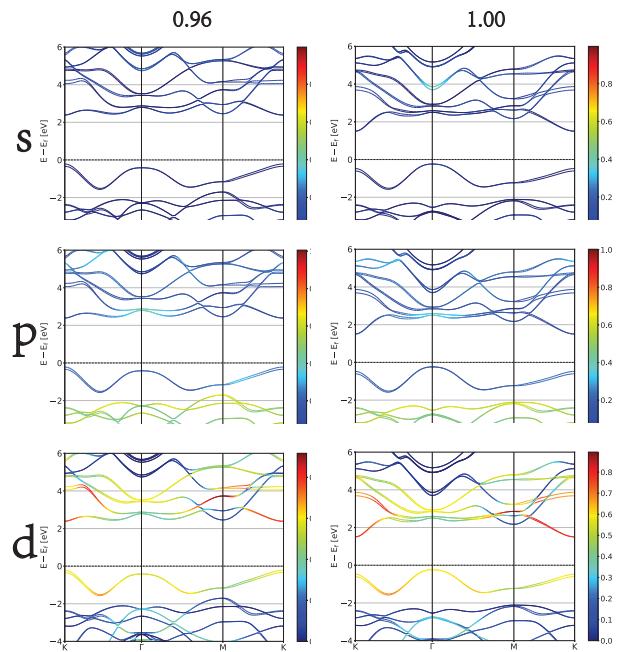

FIG. 4. (Color online) For $MoSi_2N_4$ monolayer, the orbital projected band structure at 0.96 strained and unstrained conditions.

be tuned by strain. According to orbital projected band structure, it is found that the states near the Fermi level are dominated by the Mo-d orbitals. More specifically, the states around both CBM and VBM are dominated by the Mo d_{z^2} orbital.

It is proved that the electronic structures, topological properties, transport and piezoelectric properties of 2D materials can be effectively tuned by strain[15–23,40]. The biaxial strain can be simulated by a/a_0 or $(a - a_0)/a_0$, where a and a_0 are the strained and unstrained lattice constant, respectively. The $a/a_0<1$ or $(a - a_0)/a_0<0$ means compressive strain, while $a/a_0>1$ or $(a-a_0)/a_0>0$ implies tensile strain. With a/a_0 from 0.90 to 1.10, the energy band structures are plotted in Figure 2, and the energy band gap and spin-orbit splitting value Δ at K point are shown in Figure 3.

It is found that the energy band gap firstly increases (0.90 to 0.96), and then decreases (0.96 to 1.10), which is due to transformation of CBM. Similar phenomenon can be observed in many TMD and Janus TMD monolayers[16,43]. With strain from compressive one to tensile one, the Δ has a rapid increase, and then a slight decrease. With increasing compressive strain (1.00 to 0.90), the position of CBM (VBM) changes from K (Γ) point to one point along the K-Γ direction (K point), when the compressive strain reaches about 0.94 (0.96). The compressive strain can also tune the numbers and relative positions of valence band extrema (VBE) or CBE. For example, at 0.96, the four CBE can be observed, and they energies are very close, which has very important effects on transport properties. To explore orbital contribution to the conduction bands in the case
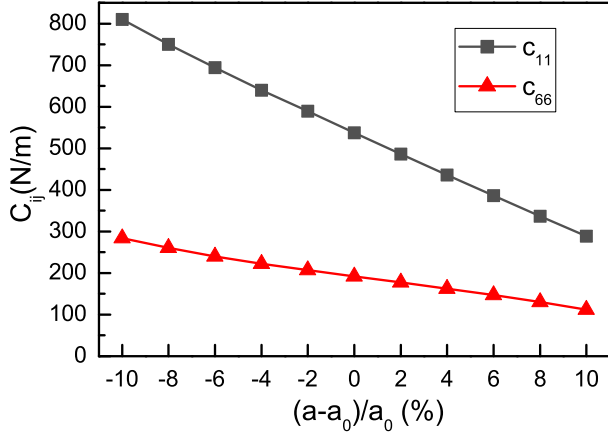
FIG. 5. (Color online) For MoSi$_2$N$_4$ monolayer, the elastic constants C_{11} and C_{66} vs a/a_0 from 0.90 to 1.10.

of 0.96 strain, we project the states to atomic orbitals at 0.96 strained and unstrained conditions, which are shown in Figure 4. At 0.96 strain, the composition of the low-energy states has little change with respect to unstrained one. At 0.98, the energy of two VBE are nearly the same. The compressive strain can make K point with spin splitting become VBM, which is very useful to allow spin manipulation for spin-valley physics. For example, at 0.94 strain, the VBM at K point is 0.49 eV higher than that at Γ point. It is clearly seen that the increasing tensile strain can make valence band around the Γ point near the Fermi level more flat.

Finally, the elastic constants C_{ij} are calculated as a function of a/a_0 to study the mechanical stability of MoSi$_2$N$_4$ monolayer with strain. For for 2D hexagonal crystals, the Born criteria of mechanical stability[44] ($C_{11} > 0$ and $C_{66} > 0$) should be satisfied. The calculated C_{11} and C_{66} as a function of strain are plotted in Figure 5, and it is clearly seen that the MoSi$_2$N$_4$ monolayer in considered strain range is mechanically stable, which is very important for farther experimental exploration.

IV. ELECTRONIC TRANSPORT PROPERTY

Proposed by Hicks and Dresselhaus in 1993[41,42], the potential thermoelectric materials can be achieved in the low-dimensional systems or nanostructures. The dimensionless figure of merit, $ZT = S^2\sigma T/(\kappa_e + \kappa_L)$, can be used to measure the efficiency of thermoelectric conversion of a thermoelectric material, where S, σ, T, κ_e and κ_L are the Seebeck coefficient, electrical conductivity, working temperature, electronic and lattice thermal conductivities, respectively. It is noted that, for the 2D material, the calculated σ, κ_e and κ_L depend on Lz (here, Lz=40 Å), and the S and ZT is independent of Lz. For 2D materials, we use electrons or holes per unit cell instead of doping concentration, which is described
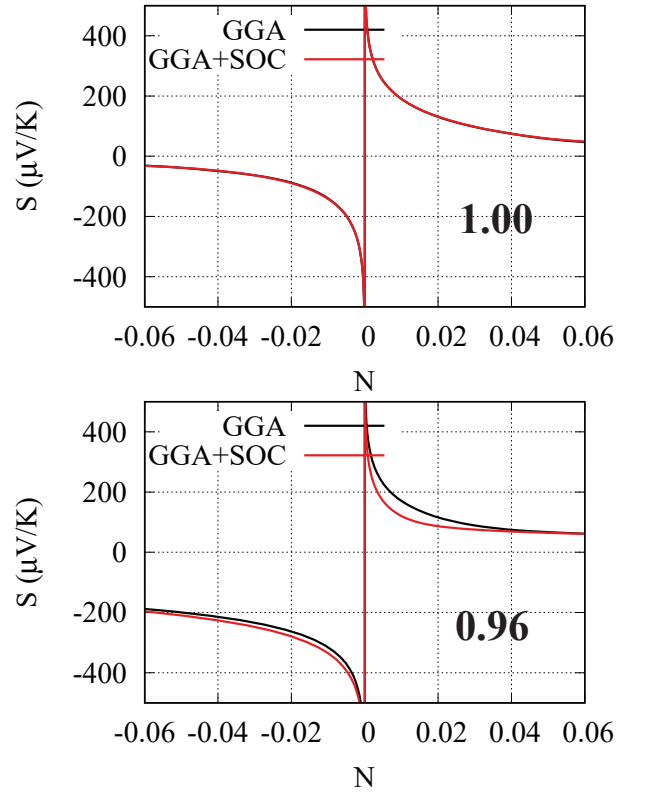

FIG. 6. (Color online) For MoSi$_2$N$_4$ monolayer, the room-temperature Seebeck coefficient S using GGA and GGA+SOC at 1.00 and 0.96 strains as a function of doping level N (The N means number of electrons or holes per unitcell).

by N, and the N $<(>)$ 0 mean n- (p-) type doping. It is proved that the SOC has important effects on transport coefficients of TMD and Janus TMD monolayers[16,18,43]. However, the SOC has neglectful influences on transport properties of unstrained MoSi$_2$N$_4$ monolayer, which can be observed from typical Seebeck coefficient S in Figure 6. This is because the energy bands near the Fermi level between GGA and GGA+SOC is nearly the same. However, the SOC has an important effect on p-type transport coefficients with the condition of compressive strain. For example at 0.96 strain, a detrimental effect on Seebeck coefficient S can be observed, when including SOC (See Figure 6). This is because the SOC can remove the band degeneracy near the VBM. So, the SOC is included to investigate the biaxial strain effects on transport coefficients of MoSi$_2$N$_4$ monolayer.

Using GGA+SOC, the room temperature S, σ/τ and $S^2\sigma/\tau$ of MoSi$_2$N$_4$ monolayer under different strain (0.90 to 1.10) are shown in Figure 7. It is clearly seen that the compressive strain has important effects on S, especially for n-type doping. However, the tensile strain produces small influences on S, especially for n-type S. These can be explained by strain-induced energy bands. When the strain is less than or equal to about 0.98, the n-type S (absolute value) can be observably improved, which is
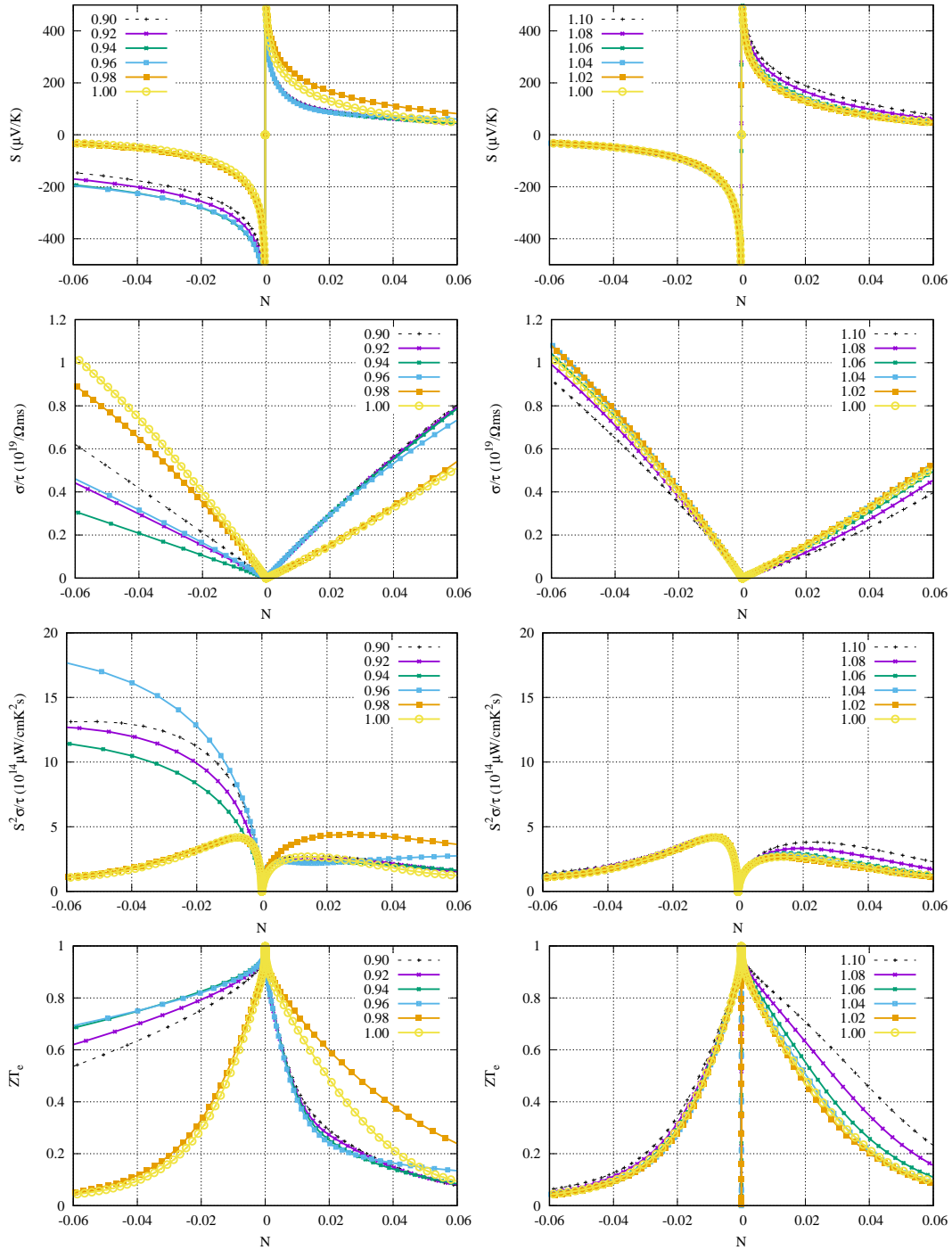
FIG. 7. (Color online) For $MoSi_2N_4$ monolayer, the room-temperature transport coefficients with the a/a_0 from 0.90 to 1.10 [(Left): compressive strain and (Right): tensile strain]: Seebeck coefficient S, electrical conductivity with respect to scattering time σ/τ, power factor with respect to scattering time $S^2\sigma/\tau$ and ZT_e (an upper limit of ZT) as a function of doping level (N) using GGA+SOC.

due to compressive strain-driven accidental conduction band degeneracies, namely bands convergence. With expanding compressive strain, in the low doping, the p-type S firstly increases, and has almost no change. This is because the valence bands convergence can be observed at about 0.98, and then is removed (At 0.98, the energy of

two VBE are nearly the same, and only one VBE near the Fermi level can be observed with compressive strain from 0.96 to 0.90.). Foe considered tensile strain, the conduction bands near the Fermi level have little change, which leads to almost unchanged n-type S. When the strain changes from 1.00 to 1.10, the p-type S increases, which

is due to tensile strain-induced more flat valence bands around Γ point near the Fermi level. This can be understood by $S = \frac{8\pi^2 K_B^2}{3eh^2} m^* T (\frac{\pi}{3n})^{2/3}$, in which m^*, T and n is the effective mass of the carrier, temperature and carrier concentration, respectively. The flat bands can produce very large effective mass of the carrier, which will lead to improved S. It is found that the strain has nearly the opposite effects on σ/τ with respect to S. It is found that the compressive strain can dramatically improve $S^2\sigma/\tau$ due to the strain-enhanced S.

An upper limit of ZT can be measured by $ZT_e = S^2\sigma T/\kappa_e$, neglecting the κ_L. The room temperature ZT_e of $MoSi_2N_4$ monolayer under different strain as a function of doping level are also shown in Figure 7. Calculated results show that the dependence of ZT_e is very similar to one of S (absolute value), which can be explained by the Wiedemann-Franz law: $\kappa_e = L\sigma T$ (L is the Lorenz number). And then the ZT_e can be reformulated by $ZT_e = S^2/L$. Thus, the strain-induced bands convergence improves S, which is beneficial to better ZT_e.

V.   CONCLUSION

In summary, we investigate the biaxial strain (0.90 to 1.10) effects on electronic structures and transport coefficients of monolayer $MoSi_2N_4$ by the reliable first-principles calculations. With the strain from 0.90 to 1.10, the energy band gap of $MoSi_2N_4$ monolayer shows a non-monotonic behavior. It is found that the SOC has little effects on transport coefficients of unstrained $MoSi_2N_4$ in considered doping range due to the hardly changed dispersion of bands near the Fermi level. However, the SOC has very important influences on transport properties of strained $MoSi_2N_4$, for example 0.96 strain, which is due to the position change of VBM. Calculated results show that compressive strain can tune the numbers and relative positions of CBE, which can lead to enhanced n-type S, and then better n-type ZT_e. Our works may provide an idea to optimize the electronic structures and transport properties of monolayer $MoSi_2N_4$.

VI.   DATA AVAILABILITY

The data that support the findings of this study are available from the corresponding author upon reasonable request.

[1] Novoselov K S et al. 2004 Science **306** 666
[2] Mak K F and Shan J 2016 Nature Photonics **10** 216
[3] Blonsky M N, Zhuang H L, Singh A K and Hennig R G 2015 ACS Nano **9** 9885
[4] Hui Z Q, Xu W X, Li X H et al. 2019 Nanoscale **11** 6045
[5] Wu W and Wang Z L 2016 Nat. Rev. Mater. **1** 16031
[6] Chhowalla M, Shin H S, Eda G, Li L J, Loh K P and Zhang H 2013 Nature Chemistry **5** 263
[7] Lu A Y, Zhu H Y, Xiao J et al. 2017 Nature Nanotechnology **12** 744
[8] Fei R X, Li W B, Li J and Yang L 2015 Appl. Phys. Lett. **107** 173104
[9] Zhang S L et al. 2016 Angew. Chem. **128** 1698
[10] Blonsky M N, Zhuang H L, Singh A K and Hennig R G 2015 ACS Nano **9** 9885
[11] Fei R X, Li W B, Li J and Yang L 2015 Appl. Phys. Lett. **107** 173104
[12] Duerloo K N, Ong M T and Reed E J 2012 J. Phys. Chem. Lett. **3** 2871
[13] Chen Y, Liu J Y, Yu J B, Guo Y G and Sun Q 2019 Phys. Chem. Chem. Phys. **21** 1207
[14] Ji J P et al. 2016 Nat. Commun. **7** 13352
[15] Lv H Y, Lu W J, Shao D F, Lub H Y and Sun Y P 2016 J. Mater. Chem. C **4** 4538
[16] Guo S D 2016 J. Mater. Chem. C **4** 9366
[17] Scalise E, Houssa M, Pourtois G, Afanas'ev V and Stesmans A 2012 Nano Res. **5** 43
[18] Guo S D 2016 Comp. Mater. Sci. **123** 8
[19] Liu H K, Qin G Z, Lin Y and Hu M 2016 Nano Lett. **16** 3831
[20] Jena N, Dimple, Behere S D and Sarkar A D 2017 J. Phys. Chem. C **121** 9181
[21] Guo S D, Guo X S, Zhang Y Y and Luo K 2020 J. Alloy. Compd. **822** 153577
[22] Dimple, Jena N, Rawat A, Ahammed R, Mohanta M K and Sarkar A D 2018 J. Mater. Chem. A **6** 24885
[23] Guo S D, Mu W Q and Zhu Y T 2021 J. Phys. Chem. Solids **151** 109896
[24] Hong Y L, Liu Z B, Wang L et al. 2020 Science **369** 670
[25] Wang L, Shi Y P, Liu M F et al. 2020 arXiv:2008.02981
[26] Guo S D, Zhu Y T, Mu W Q and Ren W C 2020 EPL **132** 57002
[27] Guo S D, Zhu Y T, Mu W Q, Wang L and Chen X Q 2021 Comp. Mater. Sci. **188** 110223
[28] Guo S D, Mu W Q, Zhu Y T and Chen X Q 2020 Phys. Chem. Chem. Phys. **22** 28359
[29] Li S, Wu W K, Feng X L et al. 2020 arXiv:2009.13253
[30] Yang C, Song Z G, Sun X T and Lu J 2020 arXiv:2010.10764
[31] Guo S D, Mu W Q, Zhu Y T, Han R Y and Ren W C 2021 J. Mater. Chem. C DOI: 10.1039/D0TC05649A (arXiv:2011.13523)
[32] Bhowmick S and Shenoy V B 2006 J. Chem. Phys. **125** 164513

[33] Kresse G 1995 J. Non-Cryst. Solids **193** 222
[34] Kresse G and Furthm*ü*ller J 1996 Comput. Mater. Sci. **6** 15
[35] Kresse G and Joubert D 1999 Phys. Rev. B **59** 1758
[36] Hohenberg P and Kohn W 1964 Phys. Rev. **136** B864; Kohn W and Sham L J 1965 Phys. Rev. **140** A1133
[37] Perdew J P, Burke K and Ernzerhof M 1996 Phys. Rev. Lett. **77** 3865
[38] Madsen G K H and Singh D J 2006 Comput. Phys. Commun. **175** 67
[39] Blaha P, Schwarz K, Madsen G K H, Kvasnicka D and Luitz J 2001 WIEN2k, an Augmented Plane Wave + Local Orbitals Program for Calculating Crystal Properties (Karlheinz Schwarz Technische University*ä*t Wien, Austria)
[40] Zhang S L, Xie M Q, Cai B et al. 2016 Phys. Rev. B **93** 245303
[41] Hicks L D and Dresselhaus M S 1993 Phys. Rev. B **47** 12727
[42] Hicks L D and Dresselhaus M S 1993 Phys. Rev. B **47** 16631(R)
[43] Guo S D and Dong J 2018 Semicond. Sci. Tech. **33** 085003
[44] Andrew R C, Mapasha R E, Ukpong A M and Chetty N 2012 Phys. Rev. B **85** 125428